

FOURIER OPTICS TREATMENT OF CLASSICAL RELATIVISTIC ELECTRODYNAMICS

G. Geloni*, E. Saldin, E. Schneidmiller and M. Yurkov,
Deutsches Elektronen-Synchrotron (DESY), Hamburg, Germany.

Abstract

We coupled Synchrotron Radiation (SR) theory with laser beam optics. In the space-frequency domain SR beams are described by solutions of the paraxial wave equation. They appear as laser beams with transverse size much larger than the wavelength. In practical situations (e.g. undulators, bends), SR beams exhibit a virtual source, similar to the waist of a laser-beam, strictly related with the inverse Fourier transform of the far-field distribution. The Fresnel formula can be used to propagate the field distribution from the waist to anywhere in space. The general theory of SR in the near-zone developed in this paper is illustrated for the special cases of undulator radiation, edge radiation and transition undulator radiation (TUR). By solving the inverse problem for the electric field we find analytical expressions for near-field distributions in terms of far-field data. A more detailed explanation of this subject is provided in [1].

INTRODUCTION

In previous works we developed a formalism ideally suited for analysis of SR problems, where we took advantage of Fourier Optics ideas [1]. Fourier Optics provides an extremely successful approach which revolutionized the treatment of wave optics problems and, in particular, laser beam optics problems. The use of Fourier Optics led us to establish basic foundations for the treatment of SR fields in terms of laser beam optics. Radiation from an ultra-relativistic electron can be interpreted as radiation from a virtual source producing a laser-like beam. The virtual source is regarded as the analogous of the waist for a laser beam, and often exhibits a plane wavefront. In this case it is specified, for any given polarization component, by a real-valued amplitude distribution of field. The laser-like representation of SR is intimately connected with the ultra-relativistic nature of the electron beam. In particular, paraxial approximation always applies. Then, free space basically acts as a spatial Fourier transformation, and the far-zone field is, aside for a phase factor, the Fourier transform of the field at any position z down the beamline. It is also, aside for a phase factor, the Fourier transform of the virtual source. Once the field at the virtual source is known, the field at other longitudinal positions, both in the far and in the near zone up to distances to the sources comparable with the radiation wavelength, can be obtained with the help of the Fresnel propagation formula. This means that the near-zone field can be calculated from the knowledge

of the far-zone field, that is possible because the paraxial approximation applies. The knowledge of the far-zone field completely specifies, through the Fresnel integral, the near-zone field as well. In the case when the electron generating the field is not ultra-relativistic, though, the paraxial approximation cannot be applied. Typically, the wavelength is comparable with the radiation formation length, and it is impossible to reconstruct the near-field distribution from the knowledge of the far-field pattern [2]. An arbitrary SR source is equivalent to several virtual sources inserted between the edges of each magnetic device. This provides conceptual insight of SR sources and should facilitate their design and analysis. In fact, since the analysis of SR sources can be reduced to that of laser-like sources, it follows that any result, method of analysis or design and any algorithm specifically developed for laser beam optics (e.g. the code ZEMAX, see [1]) is also applicable to SR sources. We first apply our method to undulator radiation around resonance. We find the field distribution of the virtual source with the help of the far-zone field distribution and we propagate to any distance of interest. Similarly, we treat edge radiation [1], studying the emission from a setup composed by a straight section and two (upstream and downstream) bends. We derive an expression for the field from a straight section that is valid at arbitrary observation position. Due to the superposition principle, this expression can be used as building block for more complicated setups. We use this idea to analyze a TUR setup consisting of an undulator preceded and followed by straight sections and bends (upstream and downstream). The first study on TUR constituted a theoretical basis for many other studies [1], dealing both with theoretical and experimental issues. More recently, TUR has been given consideration in the framework of large XFEL projects. A method was also proposed [1] to obtain intense infrared/visible light pulses naturally synchronized to x-ray pulses from the LCLS XFEL by means of Coherent TUR. In view of these applications, there is a need to extend the knowledge of TUR to the near zone. We address it here.

FAR-FIELD DATA INVERSE PROBLEM

We represent the electric field in time domain $\vec{E}(\vec{r}, t)$ as a time-dependent function of an observation point located at position $\vec{r} = \vec{r}_\perp + z\vec{z}$. In free-space, the field $\vec{E}(\vec{r}, t)$ satisfies the source-free wave equation. For monochromatic waves of angular frequency ω the wave amplitude has the form $\vec{E}_\perp(z, \vec{r}_\perp, t) = \vec{E}_\perp(z, \vec{r}_\perp) \exp[-i\omega t] + C.C.$, where the frequency ω is related to the wavelength λ by

* gianluca.aldo.geloni@desy.de

$\omega/c = 2\pi/\lambda$, and \vec{E}_\perp describes the variation of the wave amplitude in the transverse direction. \vec{E}_\perp actually represents the amplitude of the electric field in the space-frequency domain. We assume that the ultra-relativistic approximation is satisfied, that is always the case for SR setups. In this case the paraxial approximation applies [1]. This implies a slowly varying envelope of the field with respect to the wavelength. We therefore introduce $\vec{E}_\perp = \vec{E}_\perp \exp[-i\omega z/c]$. In paraxial approximation and in free space, \vec{E}_\perp obeys the paraxial wave equation along any fixed polarization component, that is $[\nabla_\perp^2 + (2i\omega/c)\partial_z]\vec{E}_\perp = 0$, where derivatives in the Laplacian operator ∇_\perp^2 are taken with respect to the transverse coordinates. Solving this equation with given initial conditions at z gives

$$\vec{E}_\perp = \frac{i\omega}{2\pi c(z_o - z)} \int d\vec{r}' \vec{E}_\perp(z, \vec{r}') \exp \left[\frac{i\omega |\vec{r}_{o\perp} - \vec{r}'|^2}{2c(z_o - z)} \right] \quad (1)$$

where the integral is performed over the transverse plane. A propagation equation for $F(z, \vec{u}) = \int d\vec{r}'_\perp \vec{E}_\perp(z, \vec{r}'_\perp) \exp[i\vec{r}'_\perp \cdot \vec{u}]$, that is the spatial Fourier transform of the field, reads instead:

$$F(z, \vec{u}) = F(z_s, \vec{u}) \exp \left[-\frac{ic|\vec{u}|^2(z - z_s)}{2\omega} \right], \quad (2)$$

where z_s is identified with the position of a virtual source. Identification of the position $z_s = 0$ with a virtual source position is always possible, but not always convenient (although often it is). From Eq. (1) and Eq. (2) a relation follows between the far-zone field distribution, dependent on the observation angle $\vec{\theta}$, and the field distribution at the virtual source position z_s :

$$\vec{E}_\perp(z_s, \vec{r}'_\perp) = \frac{i\omega z_o}{2\pi c} \int d\vec{\theta} \exp \left[-\frac{i\omega |\vec{\theta}|^2}{2c}(z_o + z_s) \right] \times \vec{E}_\perp(\vec{\theta}) \exp \left[\frac{i\omega}{c} \vec{r}'_\perp \cdot \vec{\theta} \right]. \quad (3)$$

Finally, the transverse components of the envelope of the far field can be written as [1]:

$$\vec{E}_\perp = -\frac{i\omega e}{c^2 z_o} \int_{-\infty}^{\infty} dz' \exp[i\Phi_T] \left[\left(\frac{v_x(z')}{c} - \frac{x_o}{z_o} \right) \vec{x} + \left(\frac{v_y(z')}{c} - \frac{y_o}{z_o} \right) \vec{y} \right], \quad (4)$$

where the total phase Φ_T is

$$\Phi_T = \omega \left[\frac{s(z')}{v} - \frac{z'}{c} \right] + \omega \left(\frac{1}{z_o} + \frac{z'}{z_o^2} \right)$$

$$\times \frac{[x_o - x'(z')]^2 + [y_o - y'(z')]^2}{2c} \quad (5)$$

and the charge of the electron is $(-e)$. Eq. (4) can be obtained starting directly with Maxwell's equations in the space-frequency domain. Here $v_x(z')$ and $v_y(z')$ are the horizontal and the vertical components of the transverse velocity of the electron, while $x'(z')$ and $y'(z')$ specify the transverse position of the electron as a function of the longitudinal position. Finally, we defined the curvilinear abscissa $s(z') = vt'(z')$, v being the modulus of the velocity of the electron. Eq. (4) can be used to characterize the far field from an electron moving on any trajectory as long as the ultra-relativistic approximation is satisfied. Then, once the far field is known, Eq. (3) can be used to calculate the field distribution at the virtual source. Finally, Eq. (1) solves the propagation problem at any observation position z_o . Note that part of the phase in Eq. (5) compensates with the phase in $|\vec{\theta}|^2$ in Eq. (3) at $z_s = 0$. If Eq. (4) describes a field with a spherical wavefront with center at $z = 0$, such compensation is complete. The centrum of the spherical wavefront is a privileged point, and the plane at $z = 0$ exhibits a plane wavefront. This explains why the choice $z_s = 0$ is often privileged with respect to others.

DISCUSSION

It makes sense to ask what is the range of observation positions where our algorithm applies, and what is the accuracy of our result in this range. We show that the paraxial approximation holds with good accuracy up to observation positions such that its distance d from the electromagnetic sources in the space-frequency domain, when $d \gg \lambda$. To do so, we compare results from the paraxial treatment with results without the help of the paraxial approximation. The paraxial equation must then be replaced with Helmholtz equation $c^2 \nabla^2 \vec{E} + \omega^2 \vec{E} = 4\pi c^2 \vec{\nabla} \bar{\rho} - 4\pi i\omega \vec{j}$, $\bar{\rho}(\vec{r}, \omega)$ and $\vec{j}(\vec{r}, \omega)$ being the Fourier transform of the charge density $\rho(\vec{r}, t) = -e\delta(\vec{r} - \vec{r}'(t))$ and of the current density $\vec{j}(\vec{r}, t) = -e\vec{v}(t)\delta(\vec{r} - \vec{r}'(t))$. Application of the proper Green's function yields:

$$\vec{E}(\vec{r}_o, \omega) = -\frac{i\omega e}{c} \int_{-\infty}^{\infty} dz' \frac{1}{v_z(z')} \left[\frac{\vec{\beta} - \vec{n}}{|\vec{r}_o - \vec{r}'(z')|} - \frac{ic}{\omega |\vec{r}_o - \vec{r}'(z')|^2} \right] \exp \left\{ i\omega \left[\left(\frac{s(z')}{v} - \frac{z'}{c} \right) + \left(\frac{|\vec{r}_o - \vec{r}'(z')|}{c} - \frac{z_o - z'}{c} \right) \right] \right\}. \quad (6)$$

Eq. (6) is an exact solution of Maxwell's equations with boundary conditions at infinity. The exactness of Eq. (6) allows us to control the accuracy of the paraxial approximation. A conservative estimate shows that when $d \gtrsim L_f$ this accuracy is of order $c/(\omega L_f)$, but quickly decreases as $L_f \gg d \gg c/\omega$ remaining, at least, of order of $c/(\omega d)$.

The integrand term scaling as $1/R^2$ (with $R = |\vec{r}_o - \vec{r}'(z')|$) can be dropped in Eq. (6) whenever $d \gg \lambda$. This is always the case in paraxial approximation. Note that the inverse field problem cannot be solved without application of the paraxial approximation. In this case we should solve the homogeneous Helmholtz equation with boundary conditions constituted by the knowledge of the field on an open surface (for example, a transverse plane) and additionally, Rayleigh-Sommerfeld radiation condition at infinity (separately for all polarization components). This is not enough to reconstruct the field at any position in space. However, if the paraxial approximation is applicable, the inverse field problem has a unique and stable solution. We recognize a few observation zones of interest. **Far zone.** d is such that $\vec{n} = \text{const.}$ **Formation zone.** Defined by $d \lesssim L_f$. **Radiation zone.** The field can be interpreted as radiation. **$1/R$ -zone.** The term in $1/R^2$ can be neglected in Eq. (6). **Reconstruction zone.** The inverse problem based on far-field data can be solved.

In all generality, from Eq. (6) follows that the $1/R$ -zone always coincide with the reconstruction zone. Any system of interest is characterized by a size a , a formation length L_f and the radiation wavelength λ . In the case of ultra-relativistic systems $a \gtrsim L_f \gg \lambda$. Then, the near zone is defined by $d \lesssim a$, the formation zone by $d \lesssim L_f$, the radiation zone, the reconstruction zone and the $1/R$ -zone by $d \gg (c/\omega)$. Ultra-relativistic cases present an increased level of complexity with respect to others. This complexity is at the origin of several misconceptions. Usually textbooks do not follow a direct derivation of Eq. (6). They start with the solution of Maxwell's equation in the space-time domain, the Lienard-Wiechert fields, and they apply a Fourier transformation:

$$\vec{E}(\vec{r}_o, \omega) = -e \int_{-\infty}^{\infty} dt' \left\{ \frac{\vec{n} - \vec{\beta}}{\gamma^2(1 - \vec{n} \cdot \vec{\beta})^2 R(t')^2} + \frac{\vec{n} \times [(\vec{n} - \vec{\beta}) \times \dot{\vec{\beta}}]}{c(1 - \vec{n} \cdot \vec{\beta})^2 R(t')} \right\} \exp \left[i\omega \left(t' + \frac{R(t')}{c} \right) \right] \quad (7)$$

where $\vec{\beta} = \vec{v}/c$. Inspecting Eq. (7) it looks paradoxical that the near field, including velocity and acceleration terms, can be characterized starting from the far zone, including acceleration term only. However, the magnitude of terms in $1/R^2$ and $1/R$ in Eq. (7) does not depend on λ , while that of terms in $1/R$ and $1/R^2$ in Eq. (6) does. Eq. (6) and Eq. (7) are equivalent, as can be shown by addition of the full derivative $d\Phi(t')/dt'$ of a properly chosen $\Phi(t')$ function to the integrand of Eq. (7) (and using $t' = z'/v_z(z')$). Addition of different full derivatives yields an infinite number of equivalent representations for the field, and physical sense can be ascribed to the integral only. The terms in $1/R$ and in $1/R^2$ in Eq. (6) appear as a combination of the terms in $1/R$ (acceleration term) and $1/R^2$ (velocity term) in Eq. (7). They differ from each other. As a result, there are contributions to the radiation from the velocity part in

Eq. (7). The presentation in Eq. (6) is most interesting because the magnitude of the $1/R^2$ -term in Eq. (6) can be directly compared with the magnitude of the $1/R$ -term inside the sign of integral, that is related to the $1/R$ -zone and to the reconstruction zone. If one forgets about this fact one would incorrectly conclude that far-field data cannot be used to reconstruct the field in the near-zone.

UNDULATOR LASER-LIKE SOURCE

Let us apply our algorithm in the case of undulator radiation at resonance, i.e. $\omega/(2\gamma^2 c)(1 + K^2/2) = 2\pi/\lambda_w$. Here λ_w is the undulator period, and $K = \lambda_w e H_w / (2\pi m_e c^2)$, m_e being the electron mass and H_w being the maximum of the magnetic field produced by the undulator on the z axis. Position $z = 0$ is in the undulator center. A well-known, axis-symmetric expression for the distribution of the first harmonic field $\vec{E}_\perp(z_o, \theta)$ from a planar undulator in the far-zone as a function of the observation angle θ is

$$\vec{E}_\perp = -\frac{K\omega e L_w}{c^2 z_o \gamma} A_{JJ} \exp \left[i \frac{\omega z_o}{2c} \theta^2 \right] \text{sinc} \left[\frac{\omega L_w \theta^2}{4c} \right], \quad (8)$$

where the field is polarized in the horizontal direction, $L_w = \lambda_w N_w$ is the undulator length, N_w the number of undulator periods and $A_{JJ} = J_0[K^2/(4 + 2K^2)] - J_1[K^2/(4 + 2K^2)]$, J_n being the n -th order Bessel function of the first kind. Eq. (8) describes a field with spherical wavefront centered at $z = 0$. Eq. (3) yields the field distribution at the virtual source (also axis-symmetric) [1]:

$$\vec{E}_\perp(0, r_\perp) = i \frac{K\omega e}{c^2 \gamma} A_{JJ} \left[\pi - 2\text{Si} \left(\frac{\omega r_\perp^2}{L_w c} \right) \right], \quad (9)$$

$\text{Si}(\cdot)$ being the sin integral function and r_\perp the distance from the z axis on the virtual-source plane. In laser physics, the waist is in the center of the optical cavity and the Rayleigh length is related to the resonator geometrical factor. Our virtual source is in the center of the undulator and the Rayleigh length is related to L_w . In both cases we have a plane phase front, and the transverse dimension of the waist is much larger than λ . Also, the phase of the wavefront in Eq. (9) is shifted of $-\pi/2$ with respect to the wavefront in the far zone in analogy with the Guoy phase shift. Eq. (1) gives the field at arbitrary observation position z_o :

$$\vec{E}_\perp = \frac{K\omega e A_{JJ}}{c^2 \gamma} \times \left[\text{Ei} \left(\frac{i\omega r_\perp^2}{2z_o c - L_w c} \right) - \text{Ei} \left(\frac{i\omega r_\perp^2}{2z_o c + L_w c} \right) \right] \quad (10)$$

$\text{Ei}(\cdot)$ being the exponential integral function. The field singularity at $z_o = L_w/2$ and $r_\perp = 0$ is related with the use of the resonant approximation. Introducing normalized units $\vec{r} = \sqrt{\omega/(L_w c)} \vec{r}_\perp$, $\vec{\theta} = \sqrt{\omega L_w/c} \vec{\theta}$ and $\hat{z} = z/L_w$ we obtain the intensity profile at the virtual source

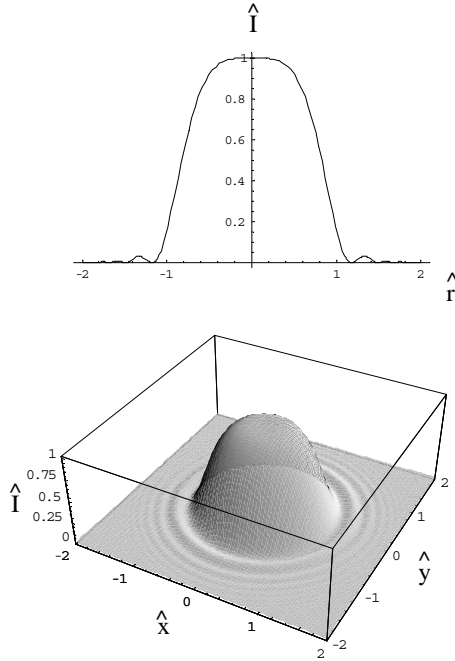
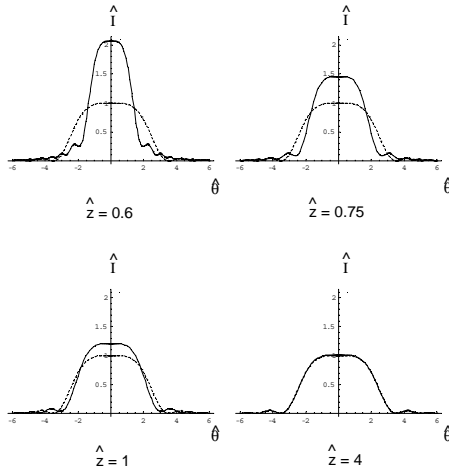
Figure 1: Intensity pattern \hat{I} at the virtual source.

Figure 2: Evolution of the intensity profile as in Eq. (12) (solid lines) compared with far field asymptotic (dashed lines).

$$\hat{I}(0, \hat{r}_\perp) = \frac{1}{\pi^2} [\pi - 2\text{Si}(\hat{r}_\perp^2)]^2, \quad (11)$$

and at any distance \hat{z}_o , both in the near and in the far zone:

$$\hat{I}(\hat{z}_o, \hat{\theta}) = \hat{z}_o^2 \left| \text{Ei}\left(\frac{i\hat{z}_o^2\hat{\theta}^2}{2\hat{z}_o - 1}\right) - \text{Ei}\left(\frac{i\hat{z}_o^2\hat{\theta}^2}{2\hat{z}_o + 1}\right) \right|^2, \quad (12)$$

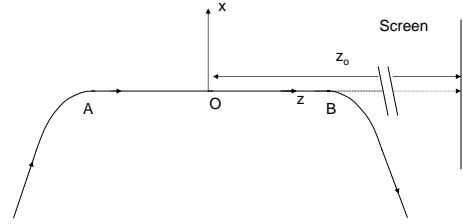


Figure 3: Edge radiation geometry.

where $\hat{\theta} = \hat{r}_\perp / \hat{z}_o$. \hat{I} at the virtual source is plotted in Fig. 1. The evolution of the intensity profile for different \hat{z}_o , Eq. (12), is given in fig. 2. A virtual source can be used as an input for wavefront propagation codes (as ZEMAX, PHASE, SRW [1]), allowing for the presence of complicate optics, likewise it has been used as an input to Eq. (1) for free-space propagation. Spontaneous SR from an electron beam can be treated as an incoherent collection of laser-like beams with different offsets and deflections (summing up the intensities), while if the electron beam is distributed coherently, radiation can be described as a coherent collection of laser-like beams.

EDGE RADIATION

We consider the system depicted in Fig. 3. An electron enters the setup via a bending magnet, passes through a straight section (segment AB) and exits the setup via another bend. Edge radiation (see references in [1]) is collected at a distance \hat{z}_o from the center of the straight section. The trajectory and, therefore, the space integration in Eq. (4) consists of the two bends b_1 and b_2 , and of the straight section AB . Let L be the length of AB . Points A and B are thus located at $z_A = -L/2$ and $z_B = L/2$. In general, one should sum the contribution due to the straight section to that from the bends. In some cases the presence of the bending magnets can be ignored as if they had zero length, and what may be called "zero-length switchers approximation" applies. Magnets act like switchers: the first magnet switches the radiation harmonic on, the second switches it off. Switchers may have different physical realizations, depending on the setup. There is no limitation to the length of the switcher. The only common feature between different switchers is that the switching process depends exponentially on the distance from the beginning of the process. Since electrodynamics is a linear theory, when the straight-section contribution cannot be considered a good approximation to the total field, it can still be considered as a fundamental building block for a more complicated setup. This justify our choice to deal with the straight-section contribution to the field only. It is interesting to discuss when the field due to switchers is negligible in our study-case. For $L \gg \gamma^2(c/\omega)$, the formation length for the straight section is $\gamma^2(c/\omega)$, while the formation length for the bend is $((c/\omega)\rho^2)^{1/3}$, ρ being the radius

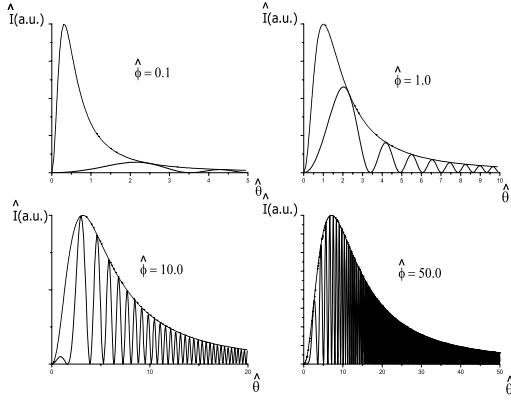


Figure 4: Directivity diagram (solid lines) of the radiation from the setup in Fig. 3 and envelope of the directivity diagram (dotted lines).

of the bend. Let the ratio between the latter and the former be $\epsilon^2 = (\lambda_c/\lambda)^{2/3} \ll 1$, where $\lambda_c = 4\pi\rho/(3\gamma^3)$ is the critical wavelength for SR and $\lambda \gg \lambda_c$, as we are interested in edge radiation. The distance $d_c = \epsilon\gamma^2(\omega/c)$ turns out to constitute an extra characteristic-length for our system. When $d \ll d_c$, the straight section contribution dominates the bending magnet one for $r_\perp > \epsilon\gamma(\omega/c)$, while for other values of r_\perp the two contributions are comparable. When $d \sim d_c$ the zero-length switcher approximation cannot be used. When $d \gg d_c$ we the straight section contribution dominates for $0 < r_\perp \ll ((\omega/c)^2\rho)^{1/3}$, the characteristic size of the radiation being $\epsilon((\omega/c)^2\rho)^{1/3}$. Finally, when $d \gg \gamma^2(\omega/c)$, the straight section contribution dominates for $0 < \theta \ll ((\omega/c)/\rho)^{1/3}$, the characteristic angle of the radiation being $\epsilon((\omega/c)/\rho)^{1/3}$.

Far field pattern of edge radiation

Field contribution calculated along the straight section. Accounting for the geometry in Fig. 3 we have $s(z') = z'$ for $z_A < z' < z_B$. Use of Eq. (4) yields the field contribution from the straight section AB :

$$\vec{E}_{AB} = \frac{i\omega eL}{c^2 z_o} \exp\left[\frac{i\omega\theta^2 z_o}{2c}\right] \vec{\theta} \operatorname{sinc}\left[\frac{\omega L}{4c}\left(\theta^2 + \frac{1}{\gamma^2}\right)\right]. \quad (13)$$

Eq. (13) describes a spherical wave and explicitly depends on L . The formation length L_{fs} for the straight section AB can be written as $L_{fs} \sim \min[\gamma^2(c/\omega), L]$. The far-zone asymptotic is independent of such value and always valid at observation positions $z_o \gg L$.

Energy spectrum of radiation. With the help of normalized quantities $\vec{\theta} = \sqrt{\omega L/c}\vec{\theta}$ and $\hat{\phi} = \omega L/(\gamma^2 c)$ we may write the directivity diagram \hat{I} of the radiation as $\hat{I} \sim \theta^2 \operatorname{sinc}^2[(\hat{\theta}^2 + \hat{\phi})/4]$. This is plotted in Fig. 4 for several values of $\hat{\phi}$ as a function of the normalized angle $\hat{\theta}$. The natural angular unit is evidently $(2\pi L/\lambda)^{-1/2}$.

There are two asymptotic cases for the problem parameter $\hat{\phi}$: $\hat{\phi} \ll 1$ and $\hat{\phi} \gg 1$. The behavior of the far-field emission is well-known in literature [1]. We take this as the starting point for investigations based on Fourier Optics.

Method of virtual sources

Edge radiation as a field from a single virtual source.

Eq. (3) and Eq. (13) yield the virtual source $\vec{E}(0, \vec{r}_\perp)$:

$$\vec{E} = -\frac{eL\omega^2}{2\pi c^3} \int d\vec{\theta} \vec{\theta} \operatorname{sinc}\left[\frac{L\omega}{4c}\left(\theta^2 + \frac{1}{\gamma^2}\right)\right] \exp\left[\frac{i\omega\vec{\theta} \cdot \vec{r}_\perp}{c}\right] \quad (14)$$

The Fourier transform in Eq. (14) is difficult to calculate analytically in full generality. An analytic expression for the field amplitude at the virtual source for $\hat{\phi} \ll 1$ reads:

$$\vec{E}(0, \vec{r}_\perp) = \frac{4\omega e}{c^2 L} \vec{r}_\perp \operatorname{sinc}\left(\frac{\omega}{Lc} |\vec{r}_\perp|^2\right). \quad (15)$$

For any value of $\hat{\phi}$, Eq. (15) explicitly depends on L , as the far-field emission does. Using $\hat{r} = \sqrt{\omega/(Lc)}\vec{r}_\perp$ the intensity pattern of the virtual source is $\hat{I}(\hat{r}) \sim \hat{r}^2 \operatorname{sinc}^2(\hat{r}^2)$ and is plotted in Fig. 5. The Fresnel formula yields the field in the near and the far zone for $\hat{\phi} \ll 1$

$$\vec{E} = -\frac{2e}{c} \frac{\vec{r}_\perp}{r_\perp^2} \exp\left[\frac{i\omega r_\perp^2}{2cz_o}\right] \left\{ \exp\left[\frac{-i\omega r_\perp^2}{2cz_o(1+2z_o/L)}\right] - \exp\left[\frac{i\omega r_\perp^2}{2cz_o(-1+2z_o/L)}\right] \right\}, \quad (16)$$

where the singular behavior at $\vec{r}_\perp = 0$ and $z_o \rightarrow L/2$ cannot be resolved within the paraxial approximation. The intensity profile associated with Eq. (16) is

$$\hat{I} = \frac{1}{\theta^2} \left| \left[\exp\left(\frac{-i\hat{\theta}^2 \hat{z}_o}{2(1+2\hat{z}_o)}\right) - \exp\left(\frac{i\hat{\theta}^2 \hat{z}_o}{2(-1+2\hat{z}_o)}\right) \right] \right|^2, \quad (17)$$

where $\hat{\theta} = \hat{r}_o/\hat{z}_o$ and $\hat{z}_o = z_o/L$. A comparison between intensity profiles at different observation points \hat{z}_o is plotted in Fig. 6. When condition $\hat{\phi} \ll 1$, studied until now, is not satisfied, the integral in Eq. (14) can be calculated numerically. The intensity distribution for the virtual source at $\hat{\phi} = 0.1$, $\hat{\phi} = 1$, $\hat{\phi} = 10$ and $\hat{\phi} = 50$ are plotted in Fig. 7. An enlarged plot of the case $\hat{\phi} = 50$ is given in Fig. 8. Fine structures are now evident, consistently with Fig. 4 for the far zone. Once the field at the virtual source is specified for any value of $\hat{\phi}$, Fourier Optics can be used to propagate it. However, we prefer to use an alternative way to solve the field propagation problem for any value of $\hat{\phi}$, capable of giving a better physical insight at $\hat{\phi} \gg 1$.

Edge radiation as a superposition of the field from two virtual sources. The far field in Eq. (13) can be written as $\vec{E}(z_o, \vec{\theta}) = \vec{E}_1(z_o, \vec{\theta}) + \vec{E}_2(z_o, \vec{\theta})$, where

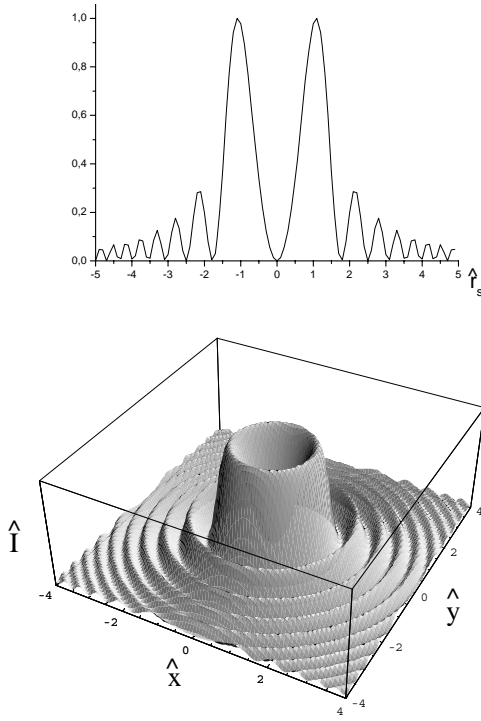


Figure 5: Intensity distribution of the virtual source, \hat{I} .

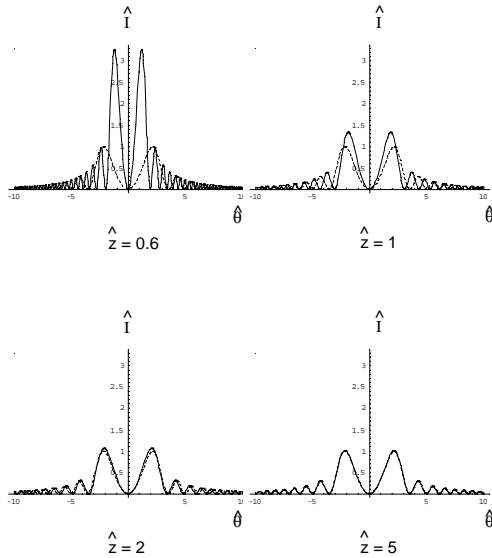


Figure 6: Evolution of the intensity profile for edge radiation for $\hat{\phi} \ll 1$ at different observation distances (solid lines) compared to the far-zone intensity (dashed lines).

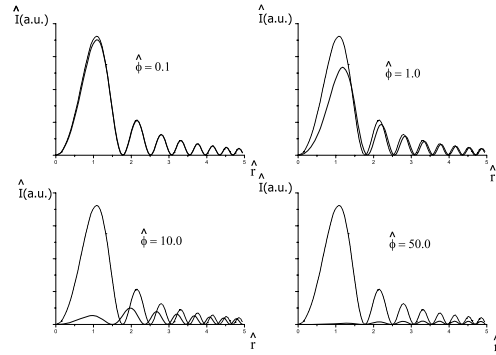


Figure 7: Intensity profiles of the virtual source for different values of $\hat{\phi}$ (solid lines) compared with the case $\hat{\phi} \ll 1$ (dotted lines).

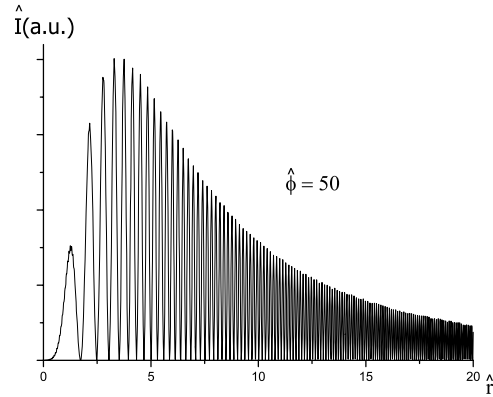


Figure 8: Intensity pattern at the virtual source for $\hat{\phi} = 50$.

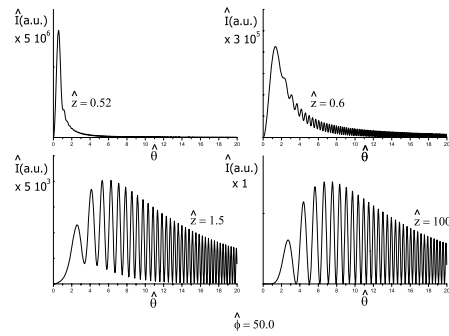


Figure 9: Edge radiation intensity profile at $\hat{\phi} = 50$ for different observation distances.

$$\begin{aligned} \vec{E}_{1,2}(\hat{z}_o, \vec{\theta}) &= \pm \frac{2e\vec{\theta}}{cz_o(\theta^2 + 1/\gamma^2)} \\ &\times \exp\left[\pm \frac{i\omega L}{4c\gamma^2}\right] \exp\left[\frac{i\omega L\theta^2}{2c}\left(\frac{z_o}{L} \pm \frac{1}{2}\right)\right]. \end{aligned} \quad (18)$$

The two terms \vec{E}_1 and \vec{E}_2 represent two spherical waves centered at $z_{s1} = L/2$ and $z_{s2} = -L/2$, corresponding to two virtual sources. Their field distribution is given by

$$\vec{E}\left(\pm \frac{L}{2}, \vec{r}_\perp\right) = \mp \frac{2ie\omega}{c^2\gamma} \exp\left[\pm \frac{i\omega L}{4c\gamma^2}\right] \frac{\vec{r}_\perp}{r_\perp} K_1\left(\frac{\omega r_\perp}{c\gamma}\right), \quad (19)$$

where $K_1(\cdot)$ is the modified Bessel function of the first order. It should be noted that Eq. (19) is identical to the well-known frequency-domain expression for the transverse component of the field from an ultra-relativistic electron moving in uniform motion. Both far zone field and the field at the virtual sources exhibit dependence on L through phase factors only. Application of the Fresnel formula allows to calculate the field at any distance z_o in frees space. Using the definition $\vec{\theta} = \vec{r}_o/\hat{z}_o$ we obtain $\hat{I} \sim |A_1 + A_2|^2$, where

$$\begin{aligned} A_{1,2} &= \mp \frac{\vec{\theta}}{\hat{\theta}} \frac{2i\sqrt{\hat{\phi}} \exp[\pm i\hat{\phi}/4]}{\hat{z}_o \mp \frac{1}{2}} \exp\left[\frac{i\hat{\theta}^2 \hat{z}_o^2}{2(\hat{z}_o \mp \frac{1}{2})}\right] \\ &\times \int_0^\infty d\xi \xi K_1(\sqrt{\hat{\phi}}\xi) J_1\left[\frac{\hat{\theta}\xi\hat{z}_o}{\hat{z}_o \mp \frac{1}{2}}\right] \exp\left[\frac{i\xi^2}{2(\hat{z}_o \mp \frac{1}{2})}\right] \end{aligned} \quad (20)$$

In Fig. 9 we plotted results for the field propagation for the case $\hat{\phi} = 50$. Radiation profiles are shown as a function of $\hat{\theta}$ at $\hat{z}_o = 0.52$, $\hat{z}_o = 0.6$, $\hat{z}_o = 1.5$ and $\hat{z}_o = 100.0$. Let us discuss the two limiting cases for $\hat{\phi} \ll 1$ and for $\hat{\phi} \gg 1$. Consider first $\hat{\phi} \ll 1$. The field at any observation distance is given by Eq. (16). There are only two observation zones of interest. **Far zone**, in the limit for $\hat{z}_o \gg 1$ and **Near zone**, when $\hat{z}_o \lesssim 1$. From Eq. (16), the total field results from the interference of the two virtual sources. The transverse size of these sources is $\gamma(c/\omega)$, independently of L . In the center of the setup instead, the virtual source has a dimension $\sqrt{(c/\omega)L}$ (see Eq. (16)). The source in the center of the setup is much smaller than those at the edge, as the two sources at the edges interfere in the center of the setup. Consider now the case $\hat{\phi} \gg 1$. Let $d_{1,2} = z_o \mp L/2$ be the distances of the observer from the edges. One can recognize four regions of interest, that are more naturally discussed in the two-source picture. **Two-edge radiation. Far zone**. When $d_{1,2} \gg L$ we are summing far field contributions from the two edge sources, see Fig. 9 for $\hat{z}_o = 100$. **Two-edge radiation. Near zone**. When $d_{1,2} \sim L$ both contributions from the sources are important, but d_1 and d_2 become sensibly different, see Fig. 9 for $\hat{z}_o = 1.5$. **Single-edge radiation. Far zone**. When $\gamma^2(c/\omega) \ll d_1 \ll L$ the

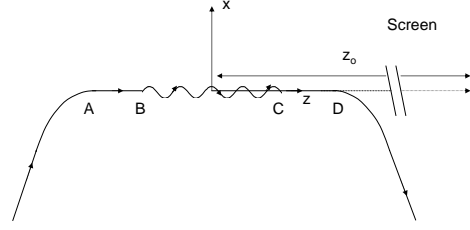


Figure 10: TUR geometry.

contribution due to the near edge is dominant, see Fig. 9 for $\hat{z}_o = 0.6$. **Single-edge radiation. Near zone**. When $0 \ll d_1 \lesssim \gamma^2(c/\omega)$ we have the near-field contribution from a single edge, and the intensity distribution tends to reproduce the behavior of the square modulus of Eq. (19). See Fig. 9 for $\hat{z}_o = 0.52$.

TRANSITION UNDULATOR RADIATION

Consider the system in Fig. 10. An electron enters the setup via a bending magnet, passes through a straight section AB , an undulator BC , and another straight section CD . Finally, it exits the setup via another bend. TUR (see references in [1]) is collected at a distance z_o from the origin of the reference system, located in the middle of the undulator. As before we ignore the presence of the bending magnets having already discussed the applicability of the "zero-length switcher approximation".

Far field pattern calculations

Field contribution from the undulator. We first consider the contribution \vec{E}_u from the undulator. We assume a planar undulator and we introduce the longitudinal Lorentz factor $\gamma_z = \gamma/(\sqrt{1 + K^2/2})$. Frequencies of interest are $\omega \ll 2\gamma_z^2 ck_w$ (with $k_w = 2\pi/\lambda_w$). As a result one obtains

$$\vec{E}_u = \frac{i\omega e}{c^2 z_o} \int_{z_B}^{z_C} dz' \exp[i\Phi_{BC}] (\theta_x \vec{x} + \theta_y \vec{y}) \quad (21)$$

with

$$\Phi_u = \omega \left[\frac{\theta_x^2 + \theta_y^2}{2c} z_o + \frac{z'}{2c} \left(\frac{1}{\gamma_z^2} + \theta_x^2 + \theta_y^2 \right) \right]. \quad (22)$$

Field contribution from the straight sections. The field contribution from a straight section has been dealt with in the previous Section. Accounting for the proper phase shift, one obtains the contributions \vec{E}_1 from AB and \vec{E}_2 from CD :

$$\vec{E}_{(1,2)} = \frac{i\omega e}{c^2 z_o} \int_{z_{(A,C)}}^{z_{(B,D)}} dz' \exp[i\Phi_{(1,2)}] (\theta_x \vec{x} + \theta_y \vec{y}) \quad (23)$$

where $\Phi_{(1,2)}$ in Eq. (23) is given by

$$\Phi_{(1,2)} = \omega \left[\frac{\theta^2}{2c} z_o - \frac{L_w}{4c\gamma_z^2} + \frac{L_w}{4c\gamma^2} + \frac{z'}{2c} \left(\frac{1}{\gamma^2} + \theta^2 \right) \right]. \quad (24)$$

Total field and energy spectrum of radiation. The contributions from the segments AB , BC and CD are:

$$\begin{aligned} \vec{E}_{(1,2)} &= \frac{i\omega e L_{(1,2)}}{c^2 z_o} \vec{\theta} \text{sinc} \left[\frac{\omega L_{(1,2)}}{4c} \left(\frac{1}{\gamma^2} + \theta^2 \right) \right] \\ &\times \exp \left[\frac{i\omega \theta^2 z_o}{2c} \right] \exp \left[-\frac{i\omega L_w}{4c} \left(\frac{1}{\gamma_z^2} + \theta^2 \right) \right] \\ &\times \exp \left[\mp \frac{i\omega L_{(1,2)}}{4c} \left(\frac{1}{\gamma^2} + \theta^2 \right) \right], \end{aligned} \quad (25)$$

$$\vec{E}_u = \frac{i\omega e L_w}{c^2 z_o} \vec{\theta} \text{sinc} \left[\frac{\omega L_w}{4c} \left(\frac{1}{\gamma_z^2} + \theta^2 \right) \right] \exp \left[\frac{i\omega \theta^2 z_o}{2c} \right] \quad (26)$$

The total field produced by the setup is obtained by summing up these contributions. The resulting energy density of radiation is known in literature [1].

Virtual source specification. Field propagation.

Eq. (25) and Eq. (26) can be interpreted as far field radiation from separate virtual sources with plane wavefronts, located at $z_{s1} = -L_w/2 - L_1/2$, $z_{su} = 0$ and $z_{s2} = L_w/2 + L_2/2$ and characterized by

$$\begin{aligned} \vec{E}_{s(1,2)} &= -\frac{\omega^2 e L_{(1,2)}}{2\pi c^3} \exp \left[\mp \frac{i\omega}{4c} \left(\frac{L_w}{\gamma_z^2} + \frac{L_{(1,2)}}{\gamma^2} \right) \right] \\ &\times \int d\vec{\theta} \vec{\theta} \text{sinc} \left[\frac{\omega L_{(1,2)}}{4c} \left(\theta^2 + \frac{1}{\gamma^2} \right) \right] \exp \left[\frac{i\omega}{c} \vec{\theta} \cdot \vec{r}_\perp \right], \end{aligned} \quad (27)$$

$$\begin{aligned} \vec{E}_{su} &= -\frac{\omega^2 e L_w}{2\pi c^3} \\ &\times \int d\vec{\theta} \vec{\theta} \text{sinc} \left[\frac{\omega L_w}{4c} \left(\theta^2 + \frac{1}{\gamma_z^2} \right) \right] \exp \left[\frac{i\omega}{c} \vec{\theta} \cdot \vec{r}_\perp \right]. \end{aligned} \quad (28)$$

L_1 , L_2 and L_w can assume different values. γ and γ_z are also different. We prescribe the same normalization for all quantities: $\vec{\theta} = \sqrt{\omega L_{\text{tot}}/c\theta}$, $\hat{\phi} = \omega L_{\text{tot}}/(\gamma^2 c)$ and $\vec{r}_\perp = \sqrt{\omega/(L_{\text{tot}}c)} \vec{r}_\perp$. Then, we introduce parameters $\hat{L}_1 = L_1/L_{\text{tot}}$, $\hat{L}_2 = L_2/L_{\text{tot}}$, $\hat{L}_w = L_w/L_{\text{tot}}$ and $\hat{\phi}_w = (\gamma^2/\gamma_z^2)\hat{\phi}$. Finally, we define $\hat{z}_s = z_s/L_{\text{tot}}$. One may check that, in the limit for $\hat{\phi} \ll 1$ and $\hat{\phi}_w \ll 1$ one obtains the same results as for edge radiation from a single straight section. A second region of interest in the parameter space that can be dealt with analytically is for $\hat{\phi} \ll 1$ and $\hat{\phi}_w \gg 1$. In this limit, the contribution from the undulator can be neglected, because the $\text{sinc}(\cdot)$ is strongly suppressed. Then, $\vec{E}(\hat{z}_{su}, \vec{r}_s) \simeq 0$, where $\vec{E} = (\omega e/c^2)\vec{E}$. The surviving virtual sources are:

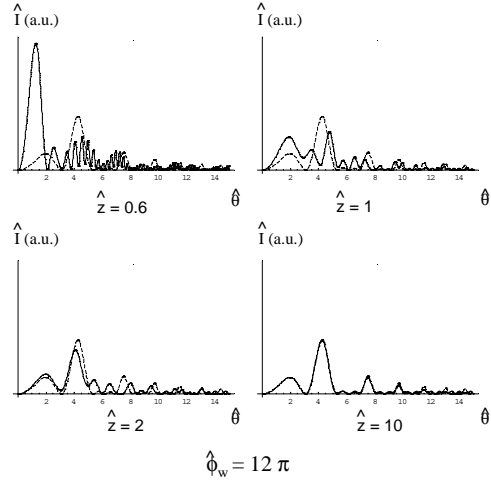


Figure 11: Evolution of the intensity profile for TUR for $\hat{\phi}_w = 12\pi$ (solid lines) and comparison with far-zone intensity (dashed lines).

$$\vec{E}_{s(1,2)} = \frac{4\vec{r}_\perp}{\hat{L}_{(1,2)}} \exp \left[-\frac{i\hat{L}_w \hat{\phi}_w}{4} \right] \text{sinc} \left(\left| \vec{r}_\perp \right|^2 / \hat{L}_1 \right). \quad (29)$$

Eq. (29) describes virtual sources characterized by plane wavefronts. Use of the Fresnel propagation formula, Eq. (1) allows reconstruction of the field in the near and in the far zone. The two surviving contributions to the field are:

$$\begin{aligned} \vec{E}_{(1,2)} &= -\frac{4\vec{r}_\perp}{\hat{r}_\perp^2} \exp \left[\mp \frac{i\hat{L}_w \hat{\phi}_w}{4} + \frac{i\hat{r}_\perp^2}{2(\hat{z}_o - \hat{z}_{s(1,2)})} \right] \\ &\times \left\{ \exp \left[-\frac{i\hat{L}_1 \hat{r}_\perp^2}{2(\hat{z}_o - \hat{z}_{s(1,2)})(\hat{L}_{(1,2)} + 2\hat{z}_o - 2\hat{z}_{s(1,2)})} \right] \right. \\ &\left. - \exp \left[\frac{i\hat{L}_{(1,2)} \hat{r}_\perp^2}{2(\hat{z}_o - \hat{z}_{s(1,2)})(-\hat{L}_{(1,2)} + 2\hat{z}_o - 2\hat{z}_{s(1,2)})} \right] \right\} \end{aligned} \quad (30)$$

Eq. (30) solves the propagation problem for the near and the far field when $\hat{\phi} \ll 1$ and $\hat{\phi}_w \gg 1$. The intensity pattern is obtained by summing up contributions in Eq. (30) and taking square modulus of the sum. To give an example we study the case $L_1 = L_2 = L_w = L_{\text{tot}}/3$. The intensity pattern periodically depends on $\hat{\phi}_w \gg 1$ with a period 12π . For illustration, in Fig. 11 we plot the intensity profile for $\hat{\phi}_w = 12\pi$ at different distances \hat{z}_o and we compare these profiles with the far field asymptote.

REFERENCES

- [1] References and a more detailed description of this subject are included in: G. Geloni, E. Saldin, E. Schneidmiller and M. Yurkov, DESY 06-127 (2006), downloadable at <http://arxiv.org/abs/physics/0608145>.
- [2] It is not so if near and formation zone do not coincide.